Beam-based impedance measurement of HL-LHC low-impedance collimators

A. Kurtulus, ^{1,2} D. Amorim, ² N. Biancacci, ² X. Buffat, ² L. Giacomel, ² J. Leuthold, ¹ N. Mounet, ² S. Redaelli, ² and J. Smajic, ¹ Institute of Electromagnetic Fields (IEF), ETH Zurich, Zurich, Switzerland, ² CERN, Geneva, Switzerland

(Received 8 April 2025; accepted 17 September 2025; published 27 October 2025)

The objective of the High Luminosity Large Hadron Collider (HL-LHC) upgrade is to attain an instantaneous luminosity that is 5 times greater than the design value of the LHC. This requires nearly 2 times higher beam intensity compared to the operational LHC value during Run 2 (2015-2018). Higher bunch intensity makes the beam more prone to coherent instabilities. To keep beam stability under control and preserve beam quality, it is therefore necessary to reduce the machine beam coupling impedance. The collimation system of the LHC is presently responsible for a significant portion of the total machine impedance budget. In this context, during the LHC long-shutdown 2 (LS2), the LHC machine has been upgraded with newly engineered low-impedance collimators whose absorbing jaws are made of molybdenum-graphite (MoGr) compared to the previously used carbon fiber composite (CFC). Secondary collimators are also coated with molybdenum (Mo) to further boost conductivity. In order to validate the benefits of the impedance reduction targeted at the collimators and to identify possible nonconformities, we performed a series of tune shift measurements on the newly installed primary and secondary collimators with LHC beams and quantified the agreement with predictions. As expected, the results show a significant reduction in the collimators' impedance contribution. Additionally, the remaining discrepancy between measurements and predictions is investigated with 3D numerical simulations by using the Wakefield Solver of Computer Simulation Technology.

DOI: 10.1103/z197-398z

I. INTRODUCTION

The Large Hadron Collider is equipped with an advanced collimation system, which consists of a series of collimators strategically placed along the accelerator ring [1]. Collimators serve as powerful shields that intercept and safely dispose particles that stray from the desired trajectories, thereby protecting sensitive machine components and maintaining the integrity of the LHC machine. The collimation system's primary objective is to prevent beaminduced machine damage from injection to flattop energy by intercepting particles that deviate from the intended trajectory, commonly known as beam halo.

One aspect of the collimation system that requires careful consideration is its impedance contribution. For any machine, detailed knowledge of the impedance of individual devices is of utmost importance, given the importance it holds in accurately predicting beam instabilities and

Published by the American Physical Society under the terms of the Creative Commons Attribution 4.0 International license. Further distribution of this work must maintain attribution to the author(s) and the published article's title, journal citation, and DOI. beam-induced heating [2]. The current collimation system accounts for over 90% of the total horizontal dipolar effective impedance at flattop [3]. Even in the HL-LHC, despite significant efforts to reduce impedance through low-impedance collimators, the collimation system still accounts for a large part of the imaginary part of the total impedance at flattop, and in particular, more than 60% at 1 GHz, where the overlap with the bunch spectrum is maximal [4].

With the upgrade of the LHC to the High Luminosity (HL-LHC), the bunch population will increase from 1.2×10^{11} to 2.3×10^{11} protons per bunch (p.p.b.) at injection [5]. Higher intensity makes the beam more prone to instabilities. This is why the collimator impedance needs to be substantially reduced to guarantee stability under various operational scenarios [6]. To decrease impedance, while keeping collimators in their nominal opening position, two possible methods can be employed. One option is to coat the collimator jaws, typically made of robust but poorly conducting materials, with a thin layer of high-conductivity coating. This improves the effective conductivity seen by the beam while preserving the device's absorbing capability. Another option is to replace the robust jaw materials with better-conducting alternatives. Both approaches effectively reduce impedance by enhancing electrical properties and optimizing beam interaction with the collimator jaws. Due to

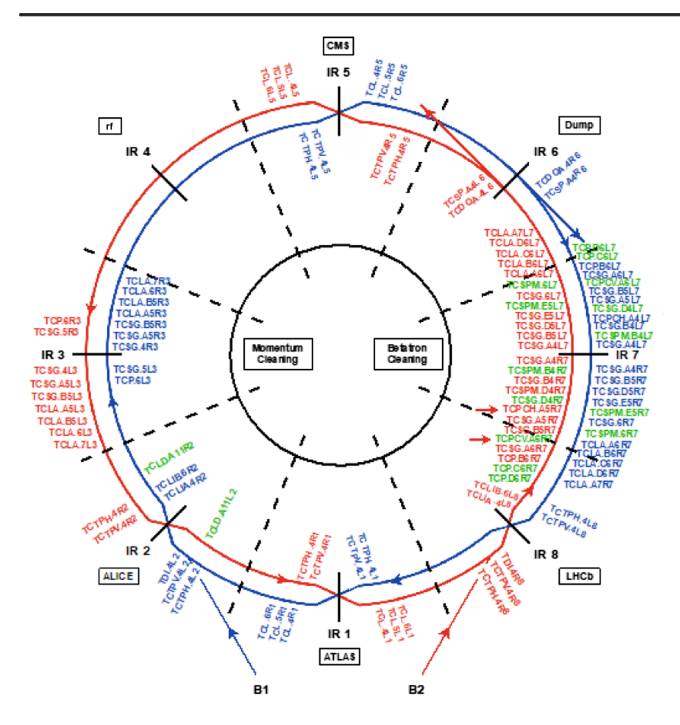


FIG. 1. LHC collimation layout including all the movable ring collimators for both beams. New HL-LHC collimators that have been added during LS2 are marked in green.

concerns regarding structural integrity during unforeseen events like single-turn losses, the latter option was regarded as unfavorable in terms of robustness [7]. In this context, several material options have been studied to reduce the impedance of HL-LHC [8].

In order to effectively mitigate losses, the jaw material of both primary (TCP) and secondary (TCS) collimators, having the largest exposure to beam-induced losses, was replaced from CFC to MoGr composite material, characterized by a factor of 5 higher dc electrical conductivity. Additionally, the secondary collimators were coated with a 5 µm layer of Mo to further boost the conductivity effectively seen by the beam. A minimum coating thickness of $5 \mu m$ is required to shield the MoGr bulk at the frequency of interest for transverse single-bunch coherent instabilities [9]. The reason for selecting Mo as a coating material is its capability to withstand the impact of the beam while maintaining adequate adherence to the MoGr substrate. The choice of the bulk material has minimal impact on impedance. However, in the event of coating damage, MoGr is preferred over CFC due to its lower resistivity.

Within the scope of the HL-LHC program, a significant upgrade took place during the LS2, between 2019 and 2021, involving the replacement of multiple CFC collimators with newly developed, low-impedance collimators. Figure 1 shows the updated layout of the LHC collimation system after LS2. Newly installed collimators are indicated in green. The description of the collimators positioned along the LHC ring is given in Table I together with their acronyms and corresponding numbers.

TABLE I. List of movable LHC ring collimators, and their description.

Collimator	Description	Number
TCP	Primary	8
TCSG/TCSP/TCSPM	Secondary	28/2/9
TCT	Tertiary	16
TCLA	Shower absorber	18
TCL	Physics debris	12
TCLD	Dispersion suppressor	2
TDI/TCLI	Injection protection	6/4
TCDQ	Dump protection	2
TCPC	Crystal collimator	4

While this study focuses on the HL-LHC collimation system, where impedance is extracted from beam-based tune shift measurements by varying collimator gaps, the fundamental principles of impedance control and beambased validation apply broadly to many high-intensity and high-brightness accelerators worldwide. In circular colliders and high-brightness linacs, collective effects such as transverse coupled-bunch instabilities, head-tail modes, and transverse mode coupling instabilities are fundamentally driven by the machine's beam coupling impedance spectrum. For facilities without movable collimators or where these devices have less impact, beam-based impedance characterization is typically performed using alternative methods such as instability growth rate analysis, tune shift measurements from various sources, and damperbased excitation techniques, which together provide critical validation of impedance models and aid in mitigating beam instabilities across diverse accelerator platforms.

The impedance of the HL-LHC collimators has been characterized at multiple production stages. First, the electrical resistivity of jaw samples was measured, followed by bench impedance tests on fully assembled collimators. After installation, beam-based measurements validate impedance performance under operational conditions. The beam-based measurements [10] typically rely on the principle that the beam-induced voltage is proportional to the beam current convolved with the machine impedance, producing measurable effects on beam parameters such as betatron tune, synchrotron frequency, and instability growth rates. In the transverse plane, a common approach is to measure tune shifts as a function of the adjustable collimator gap. The transverse impedance appears as a change in coherent tune due to the transverse kick generated by wakefields from the beam's interaction with surrounding structures. Complementary techniques, including instability growth rate measurements and damper-based excitation, allow extraction of impedance characteristics over specific frequency ranges. These methods probe the effective impedance seen by the beam, weighted over the bunch spectrum, which for the LHC typically extends up to 1 GHz due to its short (nanosecond-range) bunches.

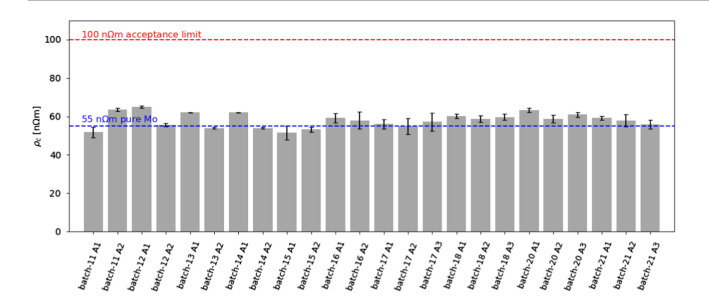


FIG. 2. Electrical resistivity of Mo-coated samples measured for different production batches.

In this context, Mo-coated MoGr was characterized using a cylindrical resonator operating in the H₀₁₁ mode [11]. The obtained results aligned closely with the theoretically predicted dc resistivity ρ_c of pure Mo and are lower than the acceptance limit of $\rho_c=100~\mathrm{n\Omega m}.$ The apparent cases where ρ_c falls slightly below the pure Mo value are within the combined uncertainty of the H₀₁₁ resonant cavity method, arising from Q_0 calibration and reproducibility of sample mounting. Figure 2, which provides an overview of electrical resistivity measurements on Mo-coated samples taken across production batches of secondary collimators, includes error bars representing this measurement uncertainty, with all measured values consistent with the theoretical value within errors. All the newly fabricated low-impedance primary and secondary collimators were systematically characterized with rf bench impedance measurements [12] which allowed to verify the device compliance for installation in the LHC.

Once installed in the machine, beam measurements were performed specifically targeting the low-impedance collimators. This benchmark process is essential for ensuring the accuracy and reliability of the impedance and the beam stability predictions made at the HL-LHC design stage.

In this work, we present the results of the beam-based impedance measurements of the newly installed low-impedance collimators. The impedance of each collimator is deduced by measuring the tune shift induced while varying the collimator aperture. The overall impedance reduction with respect to the previous CFC collimators will be presented.

This paper is organized as follows: Sec. II provides a detailed explanation of the beam-based impedance measurement procedure used to assess the collimators impedance via tune shift measurements. In Sec. III, we discuss the beam and machine parameters relevant to the measurement campaign and present the results of tune shift measurements for each measured collimator. We also compare the measurement results to the theoretical predictions obtained from analytical estimations. Furthermore, we show the improvement in terms of impedance by comparing the low-impedance collimators to their previous counterparts made of CFC material. In Sec. IV, we address the observed discrepancy between experiments and predictions by

means of 3D impedance simulations on a collimator model. The relative contribution of different parts of the collimator is progressively studied using Wakefield Solver of Computer Simulation Technology (CST) [13] providing insights into possible improvements in the way collimator impedance is modeled. Eventually, the potential impact of high order modes (HOM) on the tune shift measurement is addressed in Sec. IVA.

II. BEAM-BASED MEASUREMENT PROCEDURE

Beam-based measurements were performed to characterize the impedance of each collimator. In particular, the measurement of the tune shift variation versus collimator gap is directly correlated with the device impedance. The collimator gap can be indeed varied from its nominal position to enhance or reduce the device impedance.

The dependence of the jaw resistive wall impedance on the collimator gap g and dc resistivity ρ_c is given by

$$Z_y^{RW} \propto \sqrt{\rho_c}/g^3,$$
 (1)

while the contribution of the tapered transitions is given by [14]

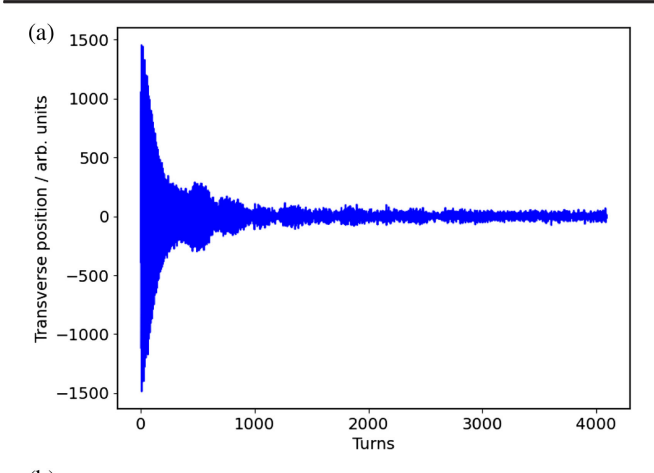
$$Z_{\nu}^{\text{Geo}} \propto 1/g^2.$$
 (2)

The resistive wall component is inversely proportional to g^3 , while the geometric component is inversely proportional to g^2 . Both the effects will be taken into account when comparing measurements to predictions in Sec. III.

Therefore, gaps larger than nominal will reduce the collimator impedance, while smaller gaps will increase it. By systematically varying the collimator gap, one can therefore deduce the collimator impedance.

From the practical point of view, the measurement process includes several steps. First, the initial tune of the beam is measured at the nominal collimator settings. Then, the gaps of selected collimators are reduced one at a time. The measured tune shift as a function of intensity is then correlated to the specific collimator moved. This correlation can then be compared to the collimator impedance model.

Dedicated measurement sessions were planned in the LHC to measure the impedance of the newly installed HL-LHC low-impedance collimators. The experiments took place on July 18, 2022 and April 17, 2023. The actual steps taken during the beam-based impedance measurements are summarized as follows: (i) A bunch with an intensity of 1.5×10^{11} (p.p.b.) was injected into each of the LHC rings, beam 1 (B1) and beam 2 (B2). The selection of the buckets was carefully made to prevent any occurrence of beambeam effects between the two beams. (ii) The beams were ramped to flattop energy (6.8 TeV). The chromaticity and octupole current were adjusted and fine-tuned to maximize the decoherence time. (iii) The bunches were coherently



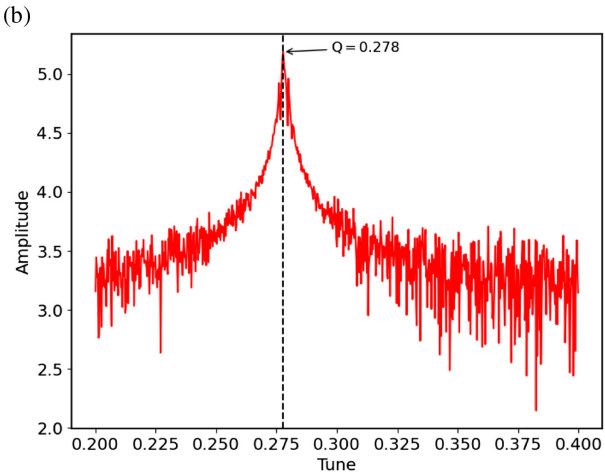


FIG. 3. Example of a turn-by-turn signal (a) and Fourier transform of the betatron oscillation shown above. The marked frequency corresponding to the tune (b).

kicked in both planes with the transverse damper (ADT) [15] while varying the collimator gap between the upper and lower limit positions. This allowed us to mitigate the effects of tune drift and tune jitters [8]. (iv) The turn-by-turn data were automatically recorded with the ADT ObsBox [16] each time an excitation was applied. (v) The data are postprocessed to obtain the tune, which is then correlated to the collimator position.

The ADT ObsBox was used to acquire the turn-by-turn transverse position data of each bunch after having been kicked. The individual tune values for each bunch are obtained by applying the Fast Fourier transformation (FFT) on the position signals. An example of the turn-by-turn bunch position data recorded with the ADT ObsBox, and the corresponding spectrum is shown in Fig. 3. To further improve the accuracy in tune determination, an iterative Fourier algorithm was used (based on Sussix [17,18]). This approach yields a more accurate result compared to the FFT when dealing with signals of short duration, as it is the case in this study.

In our configuration, the tune resolution is mainly limited by the decoherence time of the kicked oscillation,

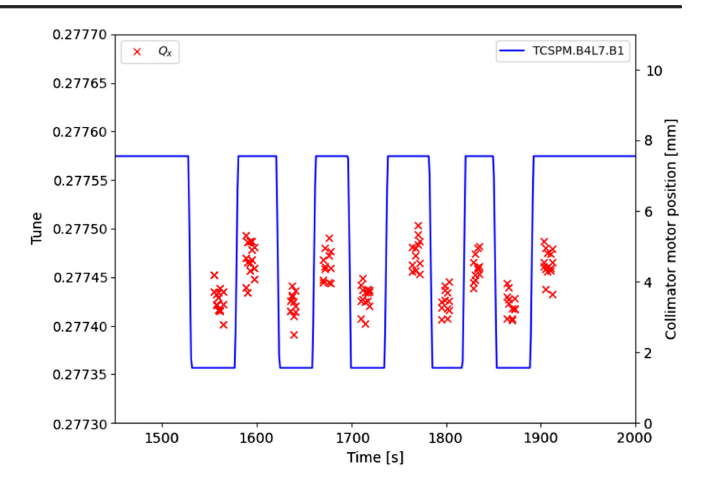


FIG. 4. Collimator position and horizontal tune versus time during the measurement of TCSPM.B4L7.B1 collimator. The solid blue line denotes the collimator's full gap motor position, and the red crosses indicate the horizontal tune computed from the kick signals.

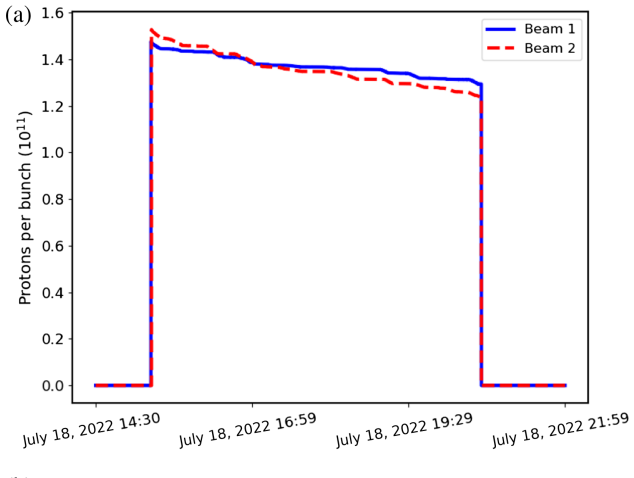
which sets the usable signal length for frequency analysis. In standard LHC operation, the strong damper gain (damping time of about 50 turns) and chromaticity (\approx 15 units) restrict the coherent signal to only a few tens of turns. For the dedicated measurements presented here, reducing the damper gain and chromaticity extended the coherent window to about 1000 turns while maintaining beam stability. Combined with the iterative Fourier analysis (Sussix/Harpy), this enables a practical tune precision of 10^{-5} , with residual limits from finite signal length, signal-to-noise ratio (SNR), and slow tune drift or jitter. When the coherent signal is shorter, the iterative Fourier approach becomes particularly beneficial, as noted above.

The collimators under investigation were cyclically opened and closed to monitor and analyze the variation in tune between the two opening positions. This method provided a tune mapping of each collimator for different jaw openings. The procedure is shown in Fig. 4 for the TCSPM.B4L7.B1 collimator, where the blue line indicates the full gap motor position of the collimator and the red points represent the measured tunes after each kick. By subtracting the tune measured at the open position from the one measured at the close position, the tune shift caused by each individual collimator is obtained. This method is applied to every collimator and summarized in Sec. III.

III. MEASUREMENT RESULTS

In this section, we provide a comprehensive presentation of the results obtained from the experiment outlined in the previous section. Figure 5 shows an overview of the beam intensity and bunch length evolution for B1 and B2, acquired during the measurement conducted on July 18, 2022.

The identical beam configuration was employed for the measurements conducted on April 17, 2023. Following



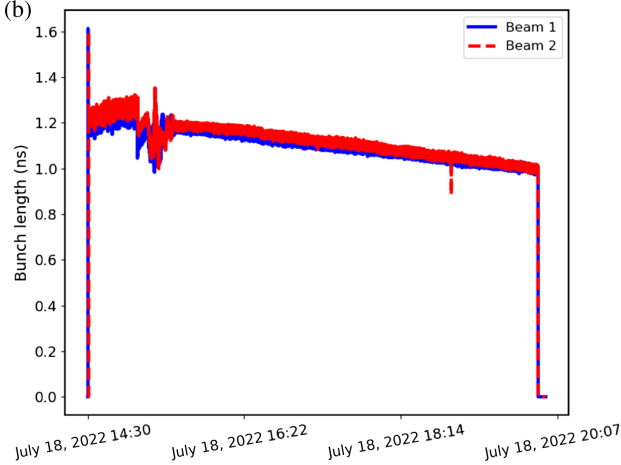


FIG. 5. Overview of beam intensity (a) and bunch length (b) evolution for B1 and B2 during the measurement.

injection, the beams were brought to top energy. At flattop, the ADT kick was synchronized and adjusted in amplitude to maximize the signal-to-noise ratio while minimizing the beam losses and unwanted scraping at the collimators.

Additionally, to attenuate the decoherence of the betatron oscillation and hence gain better resolution on the tune signal, the chromaticity was adjusted to Q' = 8, the octupole strength to 270 A, and the transverse damper gain was decreased with respect to the standard operational value. Under these settings, we observed decoherence times of about 1000 turns, compared to only a few tens of turns in standard operation with high damper gain and $Q' \approx 15$. This extended coherent window is the main enabler for the quoted tune accuracy of 10^{-5} .

Throughout the entire measurement process, a decrease of approximately 15% in beam intensity and 20% in bunch length was observed from the initial to the final stage, and these variations were incorporated into the postprocessing analysis by including the time-dependent parameters in the tune shift calculation using Eq. (3). The intensity decrease resulted from controlled excitation-related losses during the repeated ADT kicks and occasional scraping, whereas the bunch-length decrease reflects the expected synchrotron-radiation damping at 6.8 TeV during the flattop period.

The list of measured collimators is presented in Table II. All listed collimators are the ones newly installed during LS2 except TCSG.B4L7.B1 and TCSG.B4R7.B2 which are previous secondaries made of CFC. Measuring the tune shift of CFC collimators allows us to quantitatively assess the impedance reduction achieved with low-impedance collimators. An overview of the results for B1 and B2 is shown in Fig. 6, where green bars refer to tune shift measurements, while orange bars refer to the numerical expectations. These are obtained by applying Sacherer's formalism [19], which accounts for both the driving and detuning components of the LHC collimator impedance model [20].

In this framework, the coherent tune shifts are derived from the expression of the complex frequency shift of azimuthal mode m, which reads:

TABLE II. List of single collimators measured.

				Full gap (mm)
Collimator name	Family	Jaw material	Collimation plane	(Open case–closed case)
		Beam 1		
TCP.C6L7.B1	Primary	MoGr	Horizontal	2.50-4.67
TCP.D6L7.B1	Primary	MoGr	Vertical	1.78-3.34
TCSPM.B4L7.B1	Secondary	Mo-coated MoGr	Horizontal	2.56-14.52
TCSPM.6R7.B1	Secondary	Mo-coated MoGr	Horizontal	3.76-15.73
TCSG.D4L7.B1	Secondary	Mo-coated MoGr	Horizontal	1.20-10.42
TCSG.B4L7.B1	Secondary	CFC	Horizontal	2.9414.93
		Beam 2		
TCP.C6R7.B2	Primary	MoGr	Horizontal	2.49-4.61
TCP.D6R7.B2	Primary	MoGr	Vertical	1.73-3.29
TCSPM.B4R7.B2	Secondary	Mo-coated MoGr	Horizontal	2.63-14.60
TCSPM.6L7.B2	Secondary	Mo-coated MoGr	Horizontal	3.75-15.72
TCSG.B4R7.B2	Secondary	CFC	Horizontal	2.95–14.93

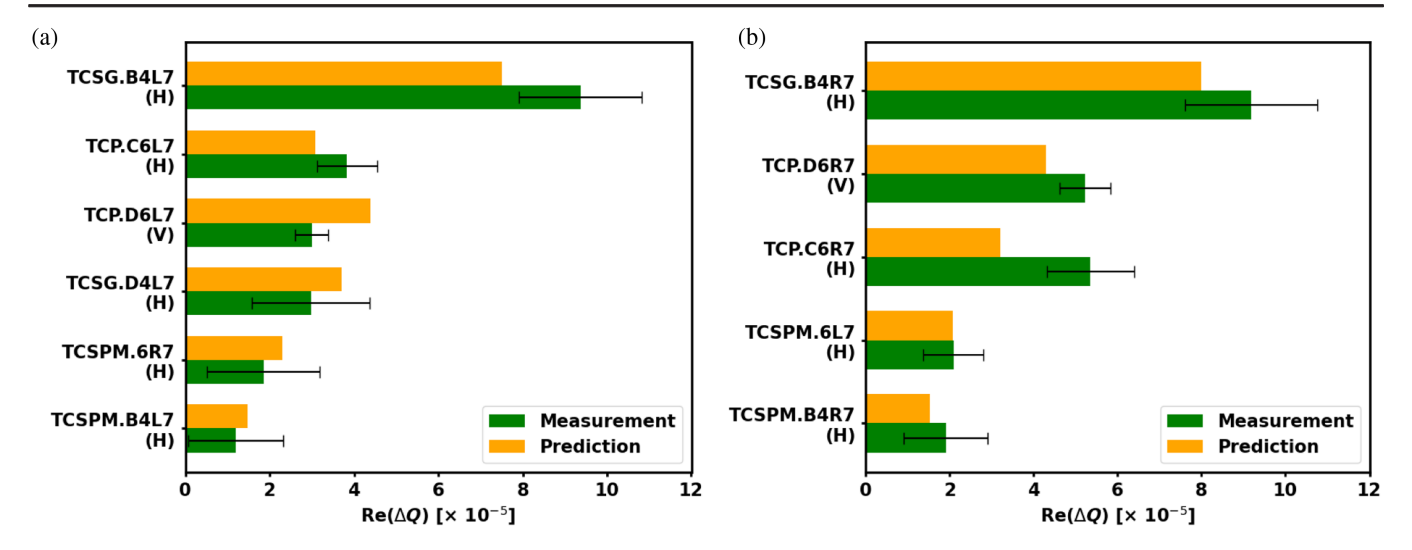


FIG. 6. Measured tune shift (green) in both horizontal (H) and vertical (V) planes of beam 1 (a) and beam 2 (b) compared to predictions from the LHC impedance model (orange).

$$(\omega_{c,m} - Q_{x0}\omega_0 - mQ_s\omega_0) = \frac{1}{|m| + 1} \frac{je^2N_b}{4\pi\gamma m_0 c Q_{x0}\tau_b} Z_{x,\text{eff}},$$
(3)

where $\omega_{c,m}$ is the complex mode frequency, Q_{x0} the unperturbed horizontal transverse tune, ω_0 the revolution frequency, Q_s the synchrotron tune, N_b the bunch population, γ the relativistic Lorentz factor, m_0 the particle mass, c the speed of light, and τ_b the full bunch length. The effective impedance $Z_{x,\text{eff}}$ encapsulates the interaction between the beam and the machine's transverse impedance spectrum. This formulation provides a first-order estimation of coherent tune shifts and serves as a direct link between the measured values and theoretical expectations.

Most measurements agree with numerical expectations within 20%–30%, with larger shifts of $\sim 10^{-4}$ for CFC collimators. The accuracy limit of the current measurement technique is $\sim 10^{-5}$, which is in line with what was achieved in previous measurements [21]. The predicted tune shift for the secondary collimators (namely TCSPM.B4L7.B1, TCSPM.B4R7.B2, and TCSG.D4L7.B1) made of Mocoated MoGr material is on the order of 10^{-5} , i.e., at the method's accuracy limit. These results confirm the Mocoated collimators' reduced impedance, at the edge of measurement accuracy.

The obtained results are generally in line with the expected values, showing a relative discrepancy ranging from 20% to 30% for both beams. Overall, the most pronounced reduction in transverse impedance is observed for the Mo-coated secondary collimators. In particular, the measured tune shift for these collimators is approximately 5 times smaller than that of the CFC secondaries, while an approximately 2.5-fold reduction is observed for the primary collimators. These observations are consistent with theoretical expectations based on the low-impedance

design of the Mo-coated materials, further confirming the effectiveness of the impedance mitigation strategy implemented during LS2.

To investigate the source of the remaining discrepancies between measurements and numerical predictions, a detailed analysis of the collimator impedance model was carried out using numerical 3D electromagnetic simulations. In particular, the Wakefield Solver of CST was employed to compute the beam-coupling impedance and to assess the contributions of different geometric and material effects. The methodology and results of this analysis, which provide further insight into the observed differences and help refine the theoretical model, are presented in the following section.

IV. MODELING OF COLLIMATOR IMPEDANCES

The expected tune shift value for each collimator is calculated with the LHC impedance and wake model [20]. Within this framework, the IW2D (or ImpedanceWake2D) code [22] is used to compute the resistive wall impedance contribution of the collimator jaws. Moreover, the geometric impedance related to the tapered transitions [14] is also computed and added to the resistive wall contribution. While this approach is often adequate and versatile [23], more detailed knowledge of the impedance is only accessible accounting for the complete device geometry [24,25]. Collimators exhibit complex geometries, incorporating features such as rf fingers, beam position monitors, and a vacuum tank designed to allow jaw movement. The current LHC impedance model does not consider these additional components, leaving room for additional impedance model improvements.

Performing 3D electromagnetic simulations on collimator CAD models offers a viable approach for the complete impedance analysis of these devices. This approach provides results that potentially better correspond to the actual

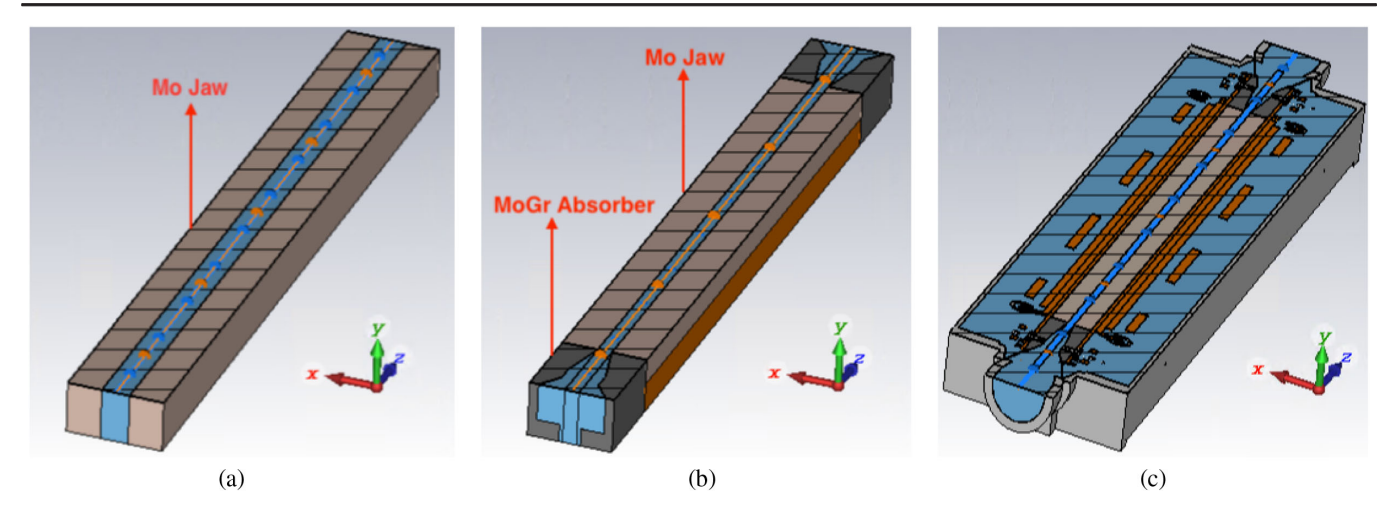


FIG. 7. Cross sections of the simulated TCSPM models. (a) Model I: the Mo jaw only. (b) Model II: both the Mo jaw and MoGr tapered absorber. (c) Model III: a more comprehensive model.

measurements, thereby enhancing the precision and confidence level of the impedance characterization.

In this regard, we methodically explore the impedance evolution of the Mo-coated TCSPM collimator by incrementally examining the relative contributions of different collimator components.

This investigation is performed by applying CST's Wakefield Solver. In this research, we consider three distinct models of the Mo-coated TCSPM collimator as shown in Fig. 7. Each one is based on components that significantly influence the device's impedance characteristics. The initial model considers solely the pure Mo jaw (model I), followed by the second model comprising both the Mo jaw and MoGr tapered absorber (model II). Finally, a more comprehensive model (e.g., accounting for beam position monitors, rf fingers, cooling pipes, jaw holders, etc.) has been developed (model III), aiming to closely mimic the actual collimators in practical applications.

During beam-based measurement, it is noteworthy to know that we maintained the physical aperture of the TCSPMs at a minimum of 1.8 mm. However, for our simulations, we chose a full physical aperture at 10 mm (i.e., with a half gap of 5 mm). This scenario is a compromise between the computational challenges associated with modeling small apertures and the actual operational collimator settings. The simulations were performed with 15 mesh lines per wavelength and an equilibrium mesh ratio of 1.5 to ensure numerical stability. Model III demands the most extensive mesh setup, involving $75 \times$ 10⁶ hexahedral mesh cells, a substantial increase compared to the 3×10^6 cells used for model I and the 5×10^6 cells employed for model II. We locally increased the mesh cell density in the beam region to allow accurate transverse wakefield simulations.

In the presented simulations, the particle beam was modeled as a longitudinal Gaussian charge distribution with rms bunch length of $\sigma_b = 75$ mm, carrying a charge of

 1×10 nC, and traveling at the speed of light. Simulations for all three scenarios covered frequencies up to 1 GHz. As expected, the most time-consuming simulations were those of model III, with each run taking approximately 27 h. These simulations were performed on a desktop PC running Windows 8 x64, featuring a 24-core Intel Xeon E5 CPU and 64 GB of RAM.

Our analysis focuses, in particular, on the driving impedances of the three different models under study. The simulation results for the three cases are shown in Fig. 8.

Initially, we performed simulations for model I and compared its results with the IW2D code. The consistency between the two approaches validated the coherence of our 3D simulation.

As a second step, model II was simulated, incorporating the MoGr tapered absorbers in addition to the elements present in model I. As expected, the real part of the impedance showed an increase, correlated to the higher resistivity of the MoGr tapered regions in comparison to the Mo jaws. Furthermore, a noticeable increase was observed in the imaginary part of the impedance, which correlated with the presence of the tapered transitions.

In the concluding phase, we simulated model III, which closely emulates the actual TCSPM collimator. In comparison to model II, the real part of the impedance remains relatively unchanged, except in the horizontal plane, where large resonance modes are observed above 800 MHz. Nevertheless, about 40% increment is observed in the imaginary part of the impedance, specifically focusing on the flat impedance regions. This aspect was initially associated with the impact of the movable rf fingers present between the MoGr tapered absorbers and the incoming/outgoing beam pipes. We conducted a detailed investigation of these transitions. The simulation results indicated that these transitions, relatively far from the beam, have a small impact on the overall impedance. Another factor that could explain the increase in the imaginary part of the

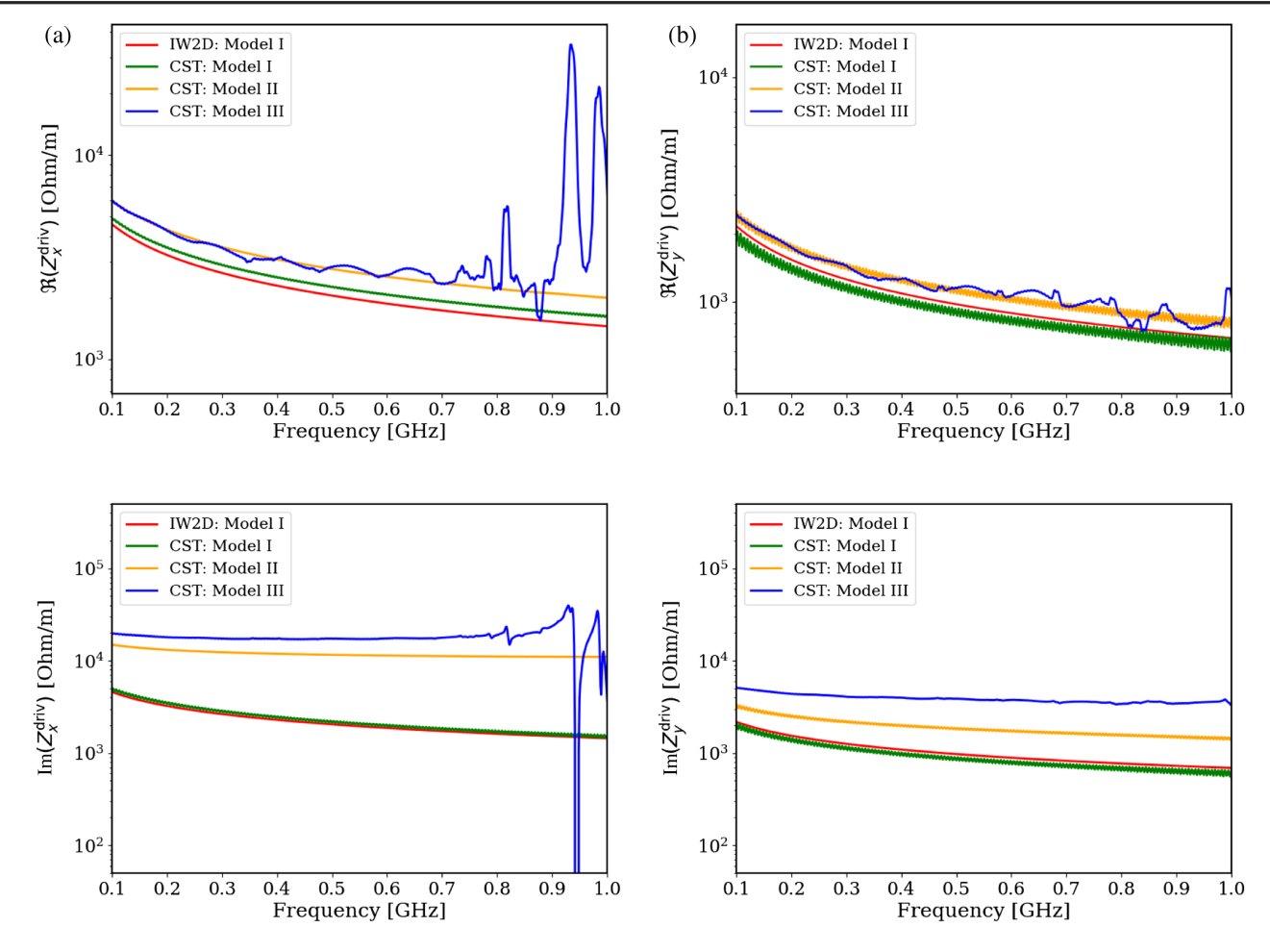
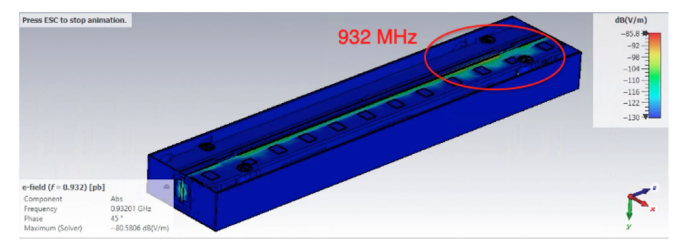


FIG. 8. The horizontal (a) and vertical (b) driving transverse impedance of a TCSPM collimator with a full gap of 10 mm as a function of frequency for the three models of the collimator jaws. The upper plots depict the real part of the impedance, while the lower plots illustrate the imaginary part.

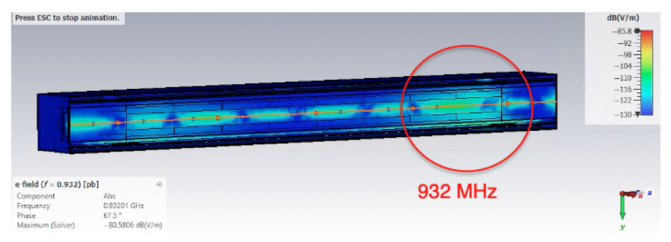
driving impedance is the presence of several higher-order modes coupled to the vacuum tank. Figure 8 shows an HOM at 932 MHz in the horizontal driving impedance, while HOMs begin to manifest in the vertical driving impedance only beyond 2 GHz. The summation of several HOM low-frequency impedances could have a measurable impact on the tune shift measurements: this subject is thoroughly addressed in the next section.

A. Investigating the higher-order modes

The analysis initially focused on the investigation of the highest HOM of the horizontal driving impedance, at a frequency of 932 MHz. CST Eigenmode simulations were performed to assess the electromagnetic field distribution within the collimator geometry. Upon inspecting the electric field distribution, we observe a significant field density between the vacuum tank and the upper plate of the collimator jaw as shown in Fig. 9(a). Further analysis revealed leakage of the mode into the beam trajectory through the lateral rf fingers, as illustrated in Fig. 9(b),



(a) Horizontal cross-section of the resonating mode.



(b) Vertical cross-section of the resonating mode.

FIG. 9. Electric field distribution of the mode at 932 MHz. (a) Horizontal cross-section of the resonating mode. (b) Vertical cross-section of the resonating mode.

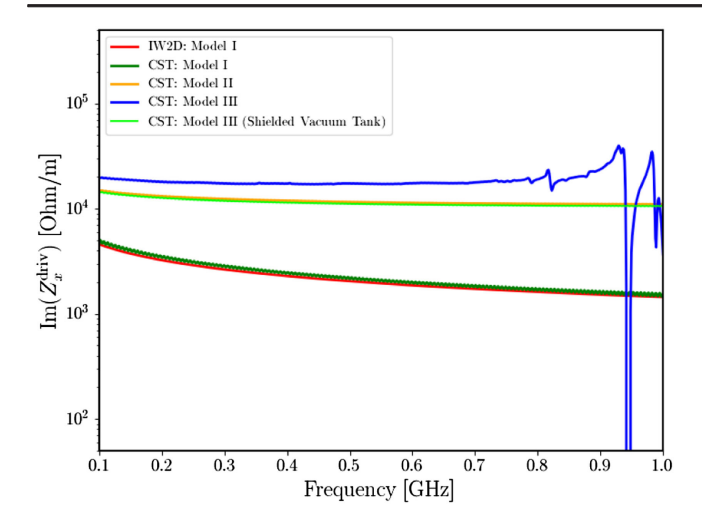


FIG. 10. The horizontal driving transverse impedance of the TCSPM collimator closing the top and bottom plates of the collimator (shielding) compared to the previous models.

thereby potentially contributing to the overall horizontal driving impedance.

Previous research [12] indicated the existence of numerous HOMs at high frequencies resonating within the vacuum tank. The low-frequency impedance of a HOM is given by the ratio of its transverse shunt impedance R and quality factor Q. While these modes generally exhibit R/Q values in the order of 100– $1000~\Omega/m$, their abundance suggests that the HOM contribution to the impedance could be significant.

To investigate this further, we performed an additional simulation by remodeling the upper and lower lateral rf fingers of the collimator jaw to prevent field leakage into the path of the beam. For this purpose, an extra metal block was added to the space at the top and bottom of the vacuum tank and collimator jaws to prevent field leakage into the path of the beam [26]. Under these conditions, all resonating modes coupling to the vacuum tank were eliminated: Fig. 10 shows the resulting driving impedance for the shielded model III (in light green) superimposing to the one of model II (yellow).

This result suggests that the discrepancy observed between measurement and simulations is related to the R/Q contribution of the collimator HOMs. Nevertheless, additional studies are required to fully characterize the HOMs, especially at the operational gaps, and quantitatively determine their overall impedance contribution.

V. CONCLUSIONS

In this study, we presented the results of beam-based impedance measurements performed on the low-impedance collimators recently installed in the LHC. We inferred the impedance of individual collimators by observing the tune shift variation versus collimator aperture. In particular, we demonstrated the secondary collimators coated with Mo

exhibit, as expected, a tune shift approximately 5 times lower than the one measured for CFC ones.

The results obtained were compared to the present LHC impedance model, revealing a difference of about 20%–30% for both B1 and B2. To investigate the discrepancy between the impedance measured in the experiment and the one predicted through theoretical calculations, a detailed 3D model of the Mo-coated TCSPM collimator was simulated with CST. This involved a step-by-step analysis on the contribution of different collimator components to the device's overall impedance. We observed a significant increase in the imaginary part of the driving impedance, amounting to nearly 40% for both horizontal and vertical planes when comparing the full collimator 3D model (model III) with the simplified one (model II) accounted for in the LHC impedance model.

The difference between the two models can be explained by accounting for the contribution of the HOMs to the impedance. In this context, we found that HOMs exhibit coupling with the vacuum tank, leaking into the beam's path through lateral rf fingers. While a quantitative analysis of the overall HOM contribution is beyond the analysis presented in this work, highlights of its potential impact on the overall horizontal driving impedance are shown: when shielding the vacuum tank by closing the top and bottom plates of the collimator, no leakage is possible and the impedance of the shielded version of model III reduces to that of model II.

Within the LHC's non-invasive-measurement constraints, further accuracy gains would primarily come from extending the coherent signal length (e.g., further optimized damper gain/chromaticity where stability permits), modestly improving SNR during the ADT excitation, and increasing averaging across repeated kicks; these knobs act directly on the decoherence- and SNR-driven limits discussed above.

Further research is planned to thoroughly characterize the HOMs and quantitatively determine their overall impedance contribution.

ACKNOWLEDGMENTS

This research has been conducted under the HL-LHC project. The authors wish to express their gratitude to P. D. Hermes, B. Lindström, L. N. Nguyen Khoi, and the LHC operation and coordination teams for their valuable support throughout the beam-based measurement process. We want to express our appreciation to the members of the ABP-CEI section and the LHC collimation team for engaging in many fruitful discussions and measurements. This work was supported by the HL-LHC project at CERN.

DATA AVAILABILITY

The data that support the findings of this article cannot be made publicly available because they contain proprietary information. The data are available upon reasonable request from the authors.

- R. W. Assmann *et al.*, The final collimation system for the LHC, CERN, Geneva, Switzerland, Report No. CERN-LHC-Project-Report-919, 2006, https://cds.cern.ch/record/ 972336.
- [2] L. Palumbo, V. G. Vaccaro, and M. Zobov, Wake fields and impedance, INFN-LNF, Frascati, Italy, Report No. LNF-94-041-P, 1995, 10.5170/CERN-1995-006.331.
- [3] L. Giacomel et al., Assessment of the real part of the impedance of the LHC collimators with instability growth rate measurements, in Proceedings of the 15th International Particle Accelerator Conference, IPAC-2024, Nashville, TN (JACoW, Geneva, Switzerland, 2024), 10.18429/JACoW-IPAC2024-THPC57.
- [4] N. Mounet, R. Tomás et al., High intensity beam dynamics assessment and challenges for HL-LHC, J. Instrum. 19, T05016 (2024).
- [5] G. Apollinari *et al.*, High-Luminosity Large Hadron Collider (HL-LHC): Technical design report V.0.1, CERN, Geneva, Switzerland, Report No. CERN-2017-007-M, 2017, 10.2172/1767028.
- [6] E. Métral *et al.*, Update of the HL-LHC operational scenarios for proton operation, Report No. CERN-ACC-NOTE-2018-0002, CERN, Geneva, Switzerland, 2018.
- [7] D. Amorim, L. Vega Cid, N. Mounet, B. Salvant, G. Mazzacano *et al.*, HL-LHC impedance and related effects, Report No. CERN-ACC-NOTE-2018-0087, CERN, Geneva, Switzerland, 2018.
- [8] S. A. Antipov *et al.*, Transverse beam stability with low-impedance collimators in the High-Luminosity Large Hadron Collider: Status and challenges, Phys. Rev. Accel. Beams **23**, 034403 (2020).
- [9] S. Antipov, Effect of collimator coating thickness on HL-LHC octupole thresholds, in *Proceedings of the 134th HSC Section Meeting* (CERN, Geneva, Switzerland, 2018), https://indico.cern.ch/event/703766/.
- [10] E. Chapochnikova, Beam-based impedance measurements, CERN Yellow Rep. School Proc. **3**, 107 (2017).
- [11] C. Accettura *et al.*, Resistivity characterization of molybdenum-coated graphite-based substrates for high-luminosity LHC collimators, Coatings **10**, 361 (2020)..
- [12] A. Kurtulus et al., Detailed electromagnetic characterisation of HL-LHC low impedance collimators, in Proceedings of the 12th International Particle Accelerator Conference, Campinas, SP, Brazil (JACoW, Geneva, Switzerland, 2021), 10.18429/JACoW-IPAC2021-THPAB235.
- [13] Computer Simulation Technology, Dassault Systèmes, CST Studio suite[®], https://www.3ds.com/products-services/simulia/ products/cst-studio-suite/.

- [14] G. Stupakov, Low frequency impedance of tapered transitions with arbitrary cross sections, Phys. Rev. ST Accel. Beams 10, 094401 (2007).
- [15] D. Valuch, Excitation by ADT and active bunch by bunch tune measurements, in *Proceedings of the 129th SPS and LHC Machine Protection Panel Meeting* (CERN, Geneva, Switzerland 2016).
- [16] M. Soderen and D. Valuch, ADT ObsBox data acquisition (LHC Beam Operation Committee, 2017), https://indico.cern.ch/event/645898.
- [17] R. Bartolini and F. Schmidt, A computer code for frequency analysis of non-linear betatron motion, Report No. CERN SL-Note-98-017-AP, CERN, Geneva, 1998, https://cds.cern.ch/record/702438.
- [18] L. Malina, Harpy: A fast, simple and accurate harmonic analysis with error propagation, in *Proceedings of the 13th International Particle Accelerator Conference, IPAC-2022, Bangkok, Thailand* (JACoW, Geneva, Switzerland, 2022), pp. 2326–2329, 10.18429/JACoW-IPAC2022-WE-POMS035.
- [19] F. Sacherer, Transverse–part II: Bunched beams, in *Proceedings of the 1st International School of Particle Accelerators "Ettore Majorana"* (1977), 10.5170/CERN-1977-013.198.
- [20] N. Mounet, LHC impedance and wake model, GitLab Repository, https://gitlab.cern.ch/IRIS/LHC_IW_model (2021).
- [21] N. Biancacci, Interpretation of wire measurements on TCSPM, in *Proceedings of the Impedance Meeting* (CERN, Geneva, Switzerland, 2017), https://indico.cern.ch/event/670910/.
- [22] N. Mounet, N. Biancacci, D. Amorim, and E. Vik, ImpedanceWake2D, https://twiki.cern.ch/twiki/bin/view/ ABPComputing/ImpedanceWake2D (2012).
- [23] N. Biancacci *et al.*, 2D and 3D collimator impedance modeling and experimental measurements, in *CERN Yellow Reports: Conference Proceedings* (CERN, Geneva, Switzerland, 2018), Vol. 1, pp. 17–23.
- [24] N. Biancacci *et al.*, Impedance simulations and measurements on the LHC collimators with embedded beam position monitors, Phys. Rev. Accel. Beams 20, 011003 (2017).
- [25] O. Frasciello *et al.*, Geometric beam coupling impedance of LHC secondary collimators, Nucl. Instrum. Methods Phys. Res., Sect. A **810**, 68 (2016).
- [26] A. Kurtulus, LHC collimators tune shift measurements and the modelling of collimator impedances, in *Proceedings of the ABP Group Information Meeting* (CERN, Geneva, Switzerland, 2023), https://indico.cern.ch/event/ 1244689/.